Effective Shape and Dynamics of Chlorophyll a in a Nematic Liquid Crystal

ARTICLE · FEBRUARY 1998

DOI: 10.1021/jp9726504 · Source: OAI

Effective Shape and Dynamics of Chlorophyll *a* in a Nematic Liquid Crystal

Alberto Arcioni,[†] Marc A. M. J. van Zandvoort,[†,‡] Paolo Bartolini,[§] Renato Torre,[§] Riccardo Tarroni,[†] Roberto Righini,[||] and Claudio Zannoni*,[†]

Dipartimento di Chimica Fisica e Inorganica, Università degli Studi di Bologna, Viale Risorgimento 4, I-40136 Bologna, Italy, LENS (European Laboratory for Non-linear Spectroscopy), Università, Largo E. Fermi 2, I-50125 Firenze, Italy, and Dipartimento di Chimica, Università, Via G. Capponi 9, I-50121 Firenze, Italy

Received: August 13, 1997; In Final Form: November 24, 1997

The ordering matrix and the three rotational diffusion tensor components of chlorophyll *a* dissolved in the nematic liquid crystal ZLI-1167 have been determined at various temperatures employing a time-dependent fluorescence depolarization technique. The axis normal to the porphyrin ring is aligned on average perpendicular to the director and exhibits the slowest tumbling with respect to the director. The phytyl chain tends to be aligned with the director, and its overall spinning is the fastest.

I. Introduction

The chlorophylls of the photosynthetic membranes of green plants play a fundamental role in light harvesting, and the study of their properties and photophysics is a fascinating area of unremitting interest in chemical physics. In the light harvesting antenna unit, constituted by a few hundred chlorophylls, each chlorophyll is embedded in the fluid lipid matrix of the thylakoid membrane (see, for example, ref 1). Structural investigations by electron[2] and X-ray[3] crystallography in various systems have shown that chlorophylls are not randomly oriented and that they are relatively far apart, separated by interdispersed lipids. On one hand this indicates the importance of a long-distance mechanism for interchlorophyll energy transfer, e.g. of Förster type.[4−6] On the other hand it underlines the importance of extending our knowledge of the ordering and dynamics of chlorophyll in anisotropic fluid matrixes. Improving our understanding of these processes should be of importance also in view of the possibility of developing artificial light harvesting units based on porphyrin ring compounds and of optimizing their efficiency (see, for example, ref 7).

The need to investigate ordered systems has prompted a number of studies of chlorophylls, and particularly of chlorophyll *a* (Chl *a*), in model systems such as poly(vinylalcohol) and nitrocellulose films, where the transition moments have been determined[8] but no dynamic information is available, lipid membranes,[9] and Langmuir−Blodgett films.[10] The photophysics of Chl *a* that determines the absorption and emission of polarized light is particularly complicated in water-containing systems because of the formation of dimers and oligomers so that the nature of the actual photoresponsive unit is not always completely clear.[11−14] Here we wish to tackle the problem of describing the order and rotational dynamics of Chl *a* in a possibly simpler model system: an oriented nematic liquid crystal. A number of studies have already been reported for Chl *a* dissolved in liquid crystals using transient EPR,[15,16] resonance Raman,[17] and fluorescence techniques,[18] particularly by the Polish school.[19−21] In these studies a number of simplifications have been necessarily employed; in particular Chl *a* has been treated as a rigid uniaxial object in its static and dynamical behavior[20] or at least in its dynamics,[16] assuming uniaxial symmetry of the rotational diffusion tensor. Moreover the temperature dependence of the order parameters has not really been determined. While these assumptions are quite justifiable in view of the complexity of the problem, they are certainly not of obvious applicability looking at the structure of Chl *a* (see Figure 1). In particular a full description would require the knowledge of the conformational distribution of the phytyl chain as well as of the porphyrin ring. Even assuming that the molecule can be considered as an effectively rigid object in the conditions of the experiment, some rather basic questions that have not yet been properly answered are the following: What is the effective shape of Chl *a*? Does its ordering matrix approximate that of a disk with the principal axis perpendicular to the porphyrin ring or rather that of a distorted rod with the long axis parallel to the phytyl chain? Moreover what is the fastest rotation axis of Chl *a*? Here we wish to tackle some of these questions, performing a series of single-photon fluorescence depolarization[22] experiments, for which we employ a fast laser source, and the experimental setup is described later. We investigate Chl *a* at different temperatures in the nematic and isotropic phase of the liquid crystal ZLI-1167,[23] previously employed by some of us in similar studies,[24] and where we may be sure, by careful preparation, that only the Chl *a* monomers are actually studied. It is clear that such a fluorescence depolarization experiment monitors only the reorientation of the transition moments, which in turn are located in the porphyrin ring. Thus on one hand the orientation and the motion we observe are also determined by that of the phytyl chain, but on the other hand, we are concentrating on an effectively rigid fragment. We then analyze the data allowing for full biaxiality of Chl *a* both in the ordering matrix and in the dynamics, using a theory, developed by two of us,[25] for the rotational diffusion of an anisotropic molecule in a liquid crystal. We shall see that this is essential to remove ambiguities in the data analysis.

* Author for correspondence.
[†] Università degli Studi di Bologna.
[‡] Present address: Debye Institute, Department of Molecular Biophysics, Buys Ballot Laboratory, Princetonplein 5, 3584 CC Utrecht, The Netherlands.
[§] LENS, Università di Firenze.
[||] Università di Firenze.

S1089-5647(97)02650-3 CCC: $15.00
Published on Web 02/06/1998

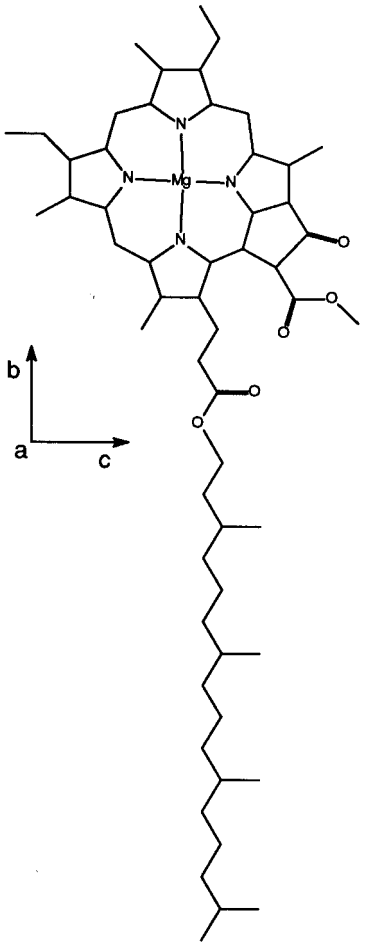

Figure 1. Structure and molecular frame of Chl *a*.

II. Experimental Section

Sample Preparation. Chlorophyll *a* was extracted from spinach leaves according to the method described by Terpstra and Lambers[26] and purified using thin-layer chromatography. A stock solution of Chl *a* in acetone (HPLC grade) was stored at −25 °C. The purity of this solution over a period of weeks was checked using isocratic reversed-phase HPLC.[27] In this way we were able to rule out the presence of optically indistinguishable Chl *a* derivatives, such as Chl *a*′ and allomerized Chl *a*.[8] The liquid crystal ZLI-1167, a ternary mixture of propyl, pentyl, and heptyl cyanocyclohexyls, i.e. *trans,trans*-4′-alkyl bicyclohexyl-4-carbonitriles, was obtained from Merck and used without further purification. The Chl *a*−acetone stock solution was used to prepare the samples, first evaporating the solvent and then mixing the fluorescent probe with the liquid crystal in the isotropic phase. All the preparations were performed under nitrogen atmosphere to avoid chlorophyll oxidation. A final concentration of Chl *a* in ZLI-1167 equal to 1×10^{-4} M was used. This concentration was chosen so as to have a high fluorescence intensity while avoiding energy-transfer depolarization effects, whose onset was observed at a concentration of about 4×10^{-4} M. The sample was held in a flat quartz cell thermostated by a oil circulation from a Lauda RCS 6-D thermostat equipped with a Lauda external controller R22 and a platinum resistance thermometer (Pt100 probe) located near the sample. The system gave a temperature stability of 0.01 K over many hours. The inner surface of the cell was coated with poly(vinylformal) and then rubbed to achieve homogeneous alignment of the liquid crystal molecules parallel to the rubbing direction. The director alignment was checked with a polarizing microscope, and it was found to be sufficiently high and uniform to give a good light extinction between cross polarizers. The thickness of the sample was also chosen so as to maximize the emission intensity while still obtaining a good alignment and having a maximum optical density of 0.2 to avoid reabsorption effects. An optimum spacing of 220 μm was found. Because of the low probe concentration, the nematic range of the mixture turned out to be essentially the same as that of the pure liquid crystal, i.e. between 32 and 83 °C.[23]

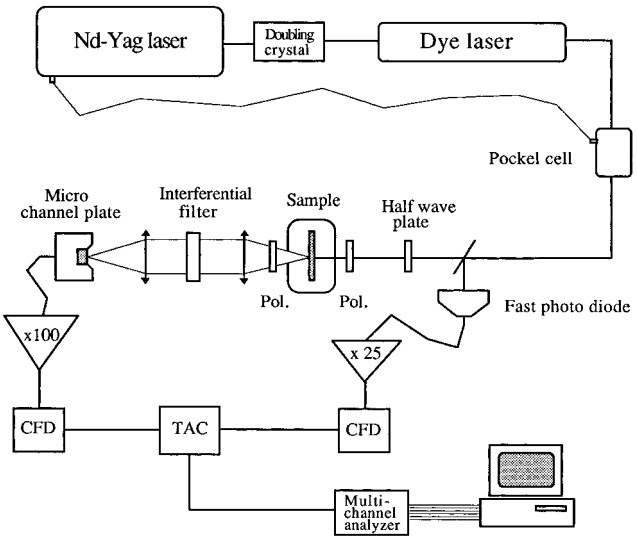

Figure 2. Experimental setup (see text for details).

Experiments. The absorption spectrum of the sample was measured with a Jasco UVIDEC-650 spectrophotometer and the maximum of absorption in the Q_Y band of chlorophyll was found at 668 nm. Excitation and emission spectra were measured with a Perkin-Elmer LS50B spectrofluorometer. The maximum of emission of the chlorophyll corresponded to a wavelength of 673 nm. From these experiments the presence of aggregates could be excluded.[8] Time-resolved fluorescence experiments were performed by means of a time-correlated single-photon-counting (TCSPC) system (see Figure 2). The laser used to excite the fluorescence probe molecules was a Coherent model 702 dye laser (pyridine 1), providing pulses about 2 ps wide with wavelength of 664 nm and energy of about 4 nJ per pulse, pumped by a mode-locked Nd:YAG laser (Coherent Antares) with a repetition rate of 76 MHz. The excited-state lifetime of chlorophyll is about 6 ns, a value in the same time range as the mode-locking period of the laser. To avoid pileup of the excitation energy, the output of the dye laser was then modulated by a Pockels cell synchronized with the pump laser, decreasing the repetition rate to 154 kHz with a contrast ratio of rejected to transmitted pulses better than 1%. This value was low enough to ensure a correct deconvolution of the fluorescence response function of the sample. The excitation radiation was then split into two beams: the first was sent to a fast photodiode, and the consequent trigger pulse was routed through an amplifier and a constant fraction discriminator (CFD) to a time-to-amplitude converter (TAC) (EG&G Ortec model 583) providing the start signal. The second beam was passed through a polarizer and sent to the sample for fluorescence excitation. The intensity of this beam was strongly attenuated up to 10 μW per pulse by means of a $\lambda/2$ plate coupled with a Glenn polarizer to prevent photochemical decomposition of the chlorophyll molecules. For the same reason the excitation spot size on the sample was expanded to 2 mm. The low excitation intensity also reduced the count rate of the detected fluorescence to about 500

counts/s, thus avoiding errors due to photoelectron superposition. The fluorescence, also polarized, was observed through a bandpass interferential filter with peak transmission at 677 nm and bandwidth of 6 nm (Omega) and a 660-nm cutoff filter (Omega). This combination of excitation and emission was selected to reach the maximum purity of the bands.[8d] Fluorescence was collected in a quasi-forward geometry, thus preventing the excitation beam from directly reaching the detection system. This consisted of an Hamamatsu R2809U-01 microchannel plate photomultiplier with transit time jitter less than 60 ps connected through a fast amplifier with 2.2-GHz bandwidth and a constant fraction discriminator to the stop input of the TAC. The instrumental function of the detection system was obtained for each experiment by measuring the time profile of the scattered laser light. For the present experimental conditions its full width at half-maximum was 80 ps. As expected for an experimental setup without emission monochromator, the sensitivity of the detection system to the vertical and horizontal polarization was essentially the same and the relative correction factor[22] was found indeed to be very close to 1. The experiments were performed in a range of temperatures from 35 to 95 °C within the aligned and isotropic phase. At every temperature the excitation polarizer was kept vertical and the emission polarizer periodically rotated, collecting for 40 s alternatively the parallel (I_{ZZ}) and the perpendicular (I_{ZX}) intensity. Typically, decay curves were measured over 650 channels with a width of 0.046 12 ns and a maximum peak height of more than 2×10^4 counts for the sum ($I_{ZZ} + 2I_{ZX}$). Due to the possibility of degradation of chlorophyll on thermal treatments and long exposure to the laser light, the photochemical stability of the sample was checked after each data acquisition run by measuring its absorption spectrum. No significant decomposition was found.

III. Theory

The probability $P(\omega)$ of finding a rigid molecule of arbitrary symmetry at an orientation given by the three Euler angles $\omega \equiv (\alpha, \beta, \gamma)$ with respect to the preferred direction (director) in a solvent with uniaxial symmetry can be expanded in a basis of Wigner rotation matrices $D^L_{0n}(\omega)$[28] as

$$P(\omega) = \frac{1}{4\pi} \sum_{Ln} (2L + 1) \langle D^{L*}_{0n} \rangle D^L_{0n}(\omega) \tag{1}$$

The averages $\langle D^L_{0n} \rangle$ are the orientational order parameters of the probe. Their number is reduced by the effective symmetry of the molecule, i.e. the set of transformations that, within the resolution of the experimental technique at hand, leaves $P(\omega)$ unchanged.[29] If only $L = 2$ properties are determined, a molecule with arbitrary symmetry will behave as a biaxial ellipsoid.

In this perspective, a more practical approach is to consider the effective potential, or potential of mean torque, acting on the probe molecule at a certain temperature T:

$$-U_{\text{probe}}(\omega, T) = k_B T \sum_{Ln} a_{Ln}(T)\, D^L_{0n}(\omega) \tag{2}$$

with k_B the Boltzmann constant. From this potential one obtains the Boltzmann expression for the distribution function:

$$P(\omega) = \frac{\exp[-U_{\text{probe}}(\omega, T)/k_B T]}{\int \exp[-U_{\text{probe}}(\omega, T)/k_B T]\, d\omega} \tag{3}$$

that can be used to calculate the probe order parameters $\langle D^L_{0n} \rangle$ as

$$\langle D^L_{0n} \rangle = \int P(\omega)\, D^L_{0n}(\omega)\, d\omega \tag{4}$$

The eigenvalues S_{ii} of the Saupe ordering matrix $\mathbf{S}$[29] can be readily obtained from the order parameters in the principal axis system as

$$S_{xx} = \frac{\sqrt{6}\langle D^2_{02} \rangle - \langle P_2 \rangle}{2} \tag{5a}$$

$$S_{yy} = -\frac{\sqrt{6}\langle D^2_{02} \rangle + \langle P_2 \rangle}{2} \tag{5b}$$

$$S_{zz} = \langle P_2 \rangle \tag{5c}$$

These principal values are invariant for any similarity transformation, including (apart from an obvious relabeling) a permutation of the molecular axis, and thus we shall find them more convenient than the $\langle D^2_{0n} \rangle$ order parameters to present our results later on. We now wish to obtain an approximate orientational distribution using maximum entropy theory,[30,31] which states that the terms entering in the definition of the potential of mean torque should be those whose average is recovered from the experiment as independent order parameters.

In general the simplest form for $U_{\text{probe}}(\omega, T)$, if uniaxial probe symmetry can be assumed, is

$$-U_{\text{probe}}(\omega, T) \equiv -U_{\text{probe}}(\beta, T) = k_B T a_{20}(T)\, P_2(\cos \beta) \tag{6}$$

which is called pure-P_2 potential and implies that the only static information that can be recovered independently is that on the order parameter $\langle P_2 \rangle$. The sign of the maximum entropy coefficient a_{20} determines whether the z axis of the probe tends to align parallel or perpendicular to the director, as expected for a molecule that is best approximated by a rod or respectively by a disk (see Figure 3).

One of the peculiarities of fluorescence depolarization experiments is the possibility of obtaining order parameters up to rank four, and thus, for a particle of effective cylindrical symmetry, we can legitimately assume also a P_2-P_4 potential,

$$-U_{\text{probe}}(\beta, T) = k_B T[a_{20}(T)\, P_2(\cos \beta) + a_{40}(T)\, P_4(\cos \beta)] \tag{7}$$

which can in principle have a minimum at a certain tilt angle. For molecules with effective biaxial symmetry, a fluorescence depolarization experiment can yield, in principle, five order parameters, i.e. $\langle P_2 \rangle$, $\langle P_4 \rangle$, $\langle D^2_{02} \rangle$, $\langle D^4_{02} \rangle$, and $\langle D^4_{04} \rangle$.[32] In practice, however, their independent determination is in most cases beyond the sensitivity of the experiment, and one has to limit the number of coefficients in the effective potential assuming, for example, the expression

$$\begin{aligned} -U_{\text{probe}}(\omega, T) \equiv -U_{\text{probe}}(\beta, \gamma, T) \\ = k_B T\{a_{20}(T)\, P_2(\cos \beta) + \\ a_{22}(T)[D^2_{02}(\beta, \gamma) + D^2_{0-2}(\beta, \gamma)]\} \end{aligned} \tag{8}$$

that is the simplest extension of eq 6 including a biaxiality contribution ($P_2-D^2_{02}$ potential). Different combinations of the order parameters $\langle P_2 \rangle$ and $\langle D^2_{02} \rangle$ or equivalently of a_{20} and a_{22} correspond to probes that can be approximated, in the axis frame that minimizes the biaxiality, as distorted disks or distorted

rods.[29b] The general theory of time-dependent depolarization in macroscopically ordered systems has been fully described elsewhere;[32,33,34] thus here we shall only recall the expressions relevant to the analysis of the present experiments. Moreover we shall consider explicitly only the case of biaxial symmetry (see eq 8), since the cylindrical limit can be easily obtained as a special one from these more general expressions by dropping all the terms containing the biaxial order parameter $\langle D^2_{02}\rangle$.

For homogeneously aligned monodomain samples, the fluorescence intensities obtained with excitation polarization aligned with the director (taken as the laboratory Z axis) and emission observed with a transparency geometry (see Figure 2) either with polarization along the Z axis (parallel intensity, $I_{ZZ}(t)$) or the X axis (perpendicular intensity, $I_{ZX}(t)$) can be expressed as

$$I_{ZZ}(t) = F(t)\left[\frac{1}{9} + \frac{1}{3}\sqrt{\frac{2}{3}}\sum_n \langle D^2_{0n}\rangle(\bar{A}^{2n*}_{\mathrm{MOL}} + A^{2n}_{\mathrm{MOL}}) + \frac{2}{3}G_0(t)\right] \quad (9)$$

$$I_{ZX}(t) = F(t)\left[\frac{1}{9} + \frac{1}{3}\sqrt{\frac{1}{6}}\sum_n \langle D^2_{0n}\rangle(2A^{2n}_{\mathrm{MOL}} - \bar{A}^{2n*}_{\mathrm{MOL}}) - \frac{1}{3}G_0(t)\right] \quad (10)$$

where $F(t)$ is the intrinsic fluorescence decay and A^{2n}_{MOL} and $\bar{A}^{2n}_{\mathrm{MOL}}$ are the irreducible spherical components, respectively of the absorption and emission transition tensors, in the molecular frame (see, for example, ref 34 for the definition of these quantities in terms of the corresponding Cartesian components). The time-dependent function $G_0(t)$, containing the dynamical information, is defined as the linear combination

$$G_0(t) = \sum_{n,n'} A^{2n}_{\mathrm{MOL}}\, \bar{A}^{2n'*}_{\mathrm{MOL}}\, \langle D^{2*}_{0n}(\omega_0)\, D^2_{0n'}(\omega_t)\rangle \quad (11)$$

where $\langle D^{2*}_{0n}(\omega_0)\, D^2_{0n'}(\omega_t)\rangle$ are orientational correlation functions evaluated, in the present work, according to the diffusional model.[25,35] Within the full biaxial model,[25] the dynamical parameters needed to calculate these functions are

$$\rho = \frac{D_x + D_y}{2} \quad (12)$$

$$\eta = \frac{2D_z}{D_x + D_y} \quad (13)$$

$$\epsilon = \frac{D_x - D_y}{D_x + D_y} \quad (14)$$

where D_x, D_y, and D_z refer to the diffusional coefficients around the molecule fixed x, y, and z axes. We recall that, in the particular case of a cylindrically symmetric diffusion tensor, $\epsilon = 0$, $\rho = D_\perp$, and $\eta = D_{\parallel}/D_\perp$, where $D_{\parallel}$ and $D_\perp$ are the diffusion coefficients around z and the axes perpendicular to z, respectively. In general we expect motion to be faster around the axis of uniaxial symmetry.

The polarization anisotropy ratio, defined as

$$r(t) = \frac{I_{ZZ}(t) - I_{ZX}(t)}{I_{ZZ}(t) + 2I_{ZX}(t)} \quad (15)$$

can be evaluated from eqs 9 and 10, obtaining

$$r(t) = \frac{\sqrt{\frac{1}{6}}\sum_n \bar{A}^{2n*}_{\mathrm{MOL}}\langle D^2_{0n}\rangle + G_0(t)}{\frac{1}{3} + \sqrt{\frac{2}{3}}\sum_n \bar{A}^{2n*}_{\mathrm{MOL}}\langle D^2_{0n}\rangle} \quad (16)$$

The anisotropy depends on order parameters and correlation functions, and thus, as we have seen, it can give some information on the effective shape of the probe. From the long time behavior of the orientational correlation functions,

$$\lim_{t\to\infty}\langle D^{2*}_{0n}(\omega_0)\, D^2_{0n'}(\omega_t)\rangle = \langle D^{2*}_{0n}\rangle\langle D^2_{0n'}\rangle \quad (17)$$

a particularly simple result for $r(\infty)$ is thus obtained:

$$r(\infty) = \sqrt{\frac{3}{2}}\sum_n \bar{A}^{2n*}_{\mathrm{MOL}}\langle D^2_{0n}\rangle \quad (18)$$

showing that this limiting plateau value is only determined by a combination of order parameters and transition moments. Equations 9 and 10 represent the idealized responses of the system to an instantaneous (δ-shaped) excitation pulse, while the observed intensities, due to the finite width of a real pulse, are a convolution of the theoretical decay with the pulse profile. In the next section we shall see how the theory outlined here in combination with a suitable deconvolution procedure can be applied to extract the available information from the experimental data.

IV. Data Analysis

The analysis of fluorescence anisotropy decays in terms of a physical model often requires an a priori guess of the effective shape of the probe in the system under study. In the simplest case one can assume probes to behave as uniaxial objects, either rod-shaped, like 1,6-diphenylhexatriene (DPH), or disk-shaped, like perylene.[34] In the case of time-dependent experiments, this means that both the ordering and diffusion tensors are assumed to be diagonal and uniaxial with respect to a common frame. Such first-order assumptions should of course be relaxed if they prove to be inadequate to fully account for the observed anisotropies. As already mentioned, a common practice is to give up the assumption of uniaxiality only on the ordering tensor. In this case the probe behaves as a biaxial object from the static point of view, but as a cylindrical one as far as dynamics is concerned. This practice is actually supported and justified by the intrinsic difficulty of recovering three independent diagonal components of the diffusion tensor, especially when two of them are fairly close, and the independent determination of all the components has been fully exploited only recently in anisotropic systems,[36,37] after a diffusion theory for fully asymmetric molecules has become available.[25] On the other hand, real probe molecules are normally neither uniaxial nor biaxial, and it is not granted that various tensors share the same principal frame. Thus in anisotropic solvents the molecular frame can always be chosen as the one giving the least biaxiality of the ordering tensor, but this is not necessarily the frame that will also give the least biaxiality in the diffusion tensor.

Chlorophyll *a* may actually fall in this last, complicated, case. Looking at the structure of the molecule in Figure 1, it is apparent that it is rather difficult to choose a priori a minimal biaxiality frame. The porphyrin ring is essentially rigid, thus an axis, say "*a*", can be taken perpendicular to the ring. A second axis, say "*b*", must be chosen in the ring plane, and a rather sensible choice is to take it parallel to the phytyl chain

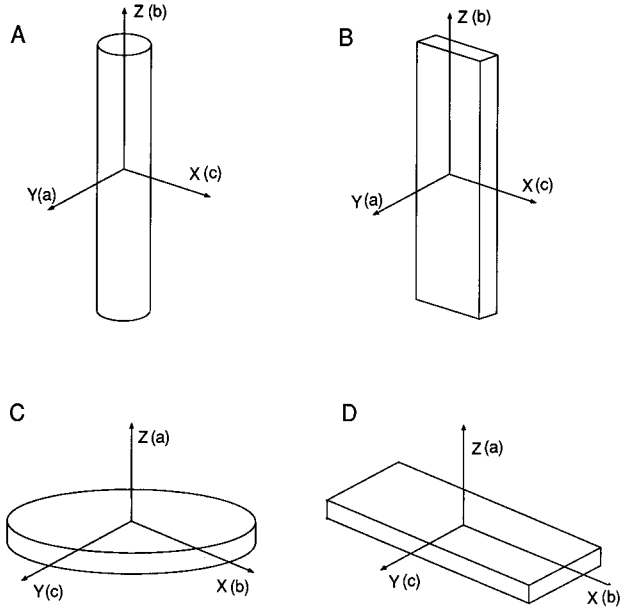

Figure 3. Effective shapes and molecular frames adopted for the models used in the analysis of the fluorescence polarization decays of Chl *a* in the liquid crystal ZLI-1167: (A) uniaxial rod; (B) biaxial rod; (C) uniaxial disk; (D) biaxial disk. In parentheses is shown the correspondence between *x*, *y*, *z* and the *a*, *b*, *c* axes of Figure 1.

in its maximum elongation, all-*trans* conformation. The third axis "*c*" is then determined as perpendicular to the other two.

On the simple basis of the amount of solvent displaced by the rotation of the molecule around *a*, *b*, and *c*, we can argue that the diffusion around *b* should be the fastest process, since it does not involve a displacement of the tail. Between the rotation around *a* and *c*, the former should be faster since it involves an in-plane movement of the porphyrin moiety within the solvent molecules.

In summary, we expect that $D_b > D_a > D_c$ (cf. Figure 1). Obviously this qualitative argument neglects conformational changes of the chain, and moreover the differences may be so small that they are blurred by the experimental noise. The most crude approximation, $D_b = D_a = D_c$, is that the molecule reorients as a spherical rotor. Other possibilities are, for example, $D_b > D_a = D_c$ and $D_b = D_c > D_a$. Similar considerations on the ordering tensor are not possible, since it is not easy to establish in advance which will be the most oriented axis.

For all the above reasons we tackled the problem of the analysis of the anisotropy decay curves from the two opposite extreme cases of prolate and oblate rotor mentioned before. Thus we have first assumed that Chl *a* behaves as a uniaxial object, either rod- or disk-shaped, with a cylindrical diffusion tensor, and next we have introduced more and more details until a convergence of the two models to the same physical picture has been obtained.

We stress that the two models should necessarily converge to a single one, the only difference being the choice of the molecular *z* axis, which coincides with *b* in the rod representation and with *a* in the disk one. The various models and the correspondence between *x*, *y*, *z* and *a*, *b*, *c* axes are summarized in Figure 3.

Our analyses have then been performed in three steps.

(1) Chl *a* is assumed to be either a rod or a disk with a prolate or oblate diffusion tensor, respectively (cylindrical model). The molecular parameters needed at each temperature are the orientations of the transition moments in the porphyrin plane (θ_{abs}, θ_{em} for the rod, ϕ_{abs}, ϕ_{em} for the disk, using polar angles), the maximum entropy parameter a_{20} entering in the pure-P_2 potential (or a_{20}, a_{40} in the P_2-P_4 model), the diffusion coefficient around the axes perpendicular to *z* ($\rho \equiv D_\perp$), and the ratio between the diffusion tensor components parallel and perpendicular to *z* ($\eta = D_\parallel/D_\perp$).

(2) We relax the assumption of uniaxiality around the *z* axis, while maintaining the diffusion tensor uniaxial with respect to that axis (restricted biaxial model). The only additional parameter required, with respect to step 1 for each temperature is a_{22}, as implied by the assumption of a $P_2-D^2_{02}$ potential.

(3) We finally remove the uniaxiality constraint also on the diffusion tensor (full biaxial model). An additional parameter with respect to step 2 is required, that is, the asymmetry ϵ of the diffusion tensor.

We notice immediately that analyses 2 and 3 are not viable, if all the new parameters are treated independently at each of the temperatures studied. Indeed a "global target"[24,32] approach, which we have previously introduced, proves essential and is implemented, in the present case, with the following assumptions.

(1) The orientations of the transition moments are fitted but assumed to be the same at all the temperatures.

(2) The diffusion tensor does not change shape with temperature and each component follows an Arrhenius-type law. This was enforced by globalizing ρ with the functional form

$$\rho(T) = \rho_0 \exp[-E_0/T] \tag{19}$$

where E_0 is in K units, while η and ϵ are fitted and forced to be equal at all the temperatures. The only abrupt change of the diffusion coefficients is allowed at the transition temperature, by fitting $\rho(T{=}95°C)$ independently (that is, it is not linked to the value at the previous temperature by the relationship eq 19).

For each choice of parameters the rotational diffusion equation is solved and the full multiexponential decays in eqs 9 and 10 are calculated and compared with the experimental ones after convolution with the instrumental pulse.

The results for the target parameters of these six analyses are summarized in Table 1. It is evident from the global reduced χ^2 that the simple uniaxial pure-P_2 model, either rod or disk, can readily describe most of the features of the anisotropy decays. However, the ordering tensor components S_{aa}, S_{bb}, and S_{cc}, obtained from either the rod or the disk model, are at best in qualitative agreement with each other. For example, at $T =$ 35 °C, $S_{bb} = 0.317$, $S_{aa} = S_{cc} = -0.159$ for the rod and $S_{bb} = S_{cc} = 0.243$, $S_{aa} = -0.486$ for the disk. Using the P_2-P_4 model somewhat improves the overall χ^2 but leaves essentially the same disagreement between the S_{ii} components.

We now turn to the second step: attempting to remove the uniaxiality approximation in the ordering matrix alone. We notice first (see columns 3 and 6 of Table 1) that the inclusion of biaxiality in the ordering tensor alone decreases the value of the global reduced χ^2 significantly and that the agreement between the two approaches is considerably improved. In particular we find from both models that, at all the temperatures, *a* is the most oriented axis, indicating that, from the orientational point of view, Chl *a* is best described as a distorted disk oriented perpendicular to the nematic director (e.g., at $T = 35$ °C, $\langle P_2 \rangle = -0.450$), rather than a distorted rod (e.g., at $T = 35$ °C, $\langle P_2 \rangle = 0.486$).

We see (column 3 of Table 1) that when allowing for the biaxiality in **S**, the decrease of the global reduced χ^2 is even more pronounced for the rod model, suggesting that the true diffusion tensor of Chl *a* is best approximated by a cylindrical

TABLE 1: Target Parameters and Reduced χ^2 for the Global Analyses (See Text)

	rod			disk		
		biaxial			biaxial	
	uniaxial	restricted	full	uniaxial	restricted	full
θ_{abs}/°	48 ± 1	68 ± 1	68 ± 2	90	90	90
θ_{em}/°	23 ± 1	43 ± 1	43 ± 1	90	90	90
ϕ_{abs}/°	0	0	0	0	64 ± 2	67 ± 2
ϕ_{em}/°	0	0	0	20.3 ± 0.1	39 ± 2	42 ± 1
$a_{20}(35)$	1.42 ± 0.01	3.78 ± 0.46	3.88 ± 0.52	−34.97 ± 2.12	−9.92 ± 3.45	−12.44 ± 4.85
$a_{22}(35)$	0	6.31 ± 1.12	6.54 ± 1.33	0	0.77 ± 0.15	0.87 ± 0.18
$a_{20}(40)$	1.45 ± 0.02	4.11 ± 0.59	4.25 ± 0.67	−34.27 ± 2.52	−10.13 ± 3.73	−13.33 ± 5.82
$a_{22}(40)$	0	7.35 ± 1.48	7.69 ± 1.73	0	0.77 ± 0.15	0.84 ± 0.18
$a_{20}(45)$	1.41 ± 0.02	3.76 ± 0.46	3.90 ± 0.53	−17.13 ± 0.58	−7.01 ± 1.72	−8.90 ± 2.51
$a_{22}(45)$	0	6.50 ± 1.15	6.86 ± 1.34	0	0.89 ± 0.14	0.95 ± 0.16
$a_{20}(50)$	1.30 ± 0.02	3.15 ± 0.29	3.24 ± 0.32	−8.72 ± 0.14	−5.48 ± 0.89	−6.44 ± 1.07
$a_{22}(50)$	0	5.52 ± 0.72	5.78 ± 0.81	0	0.75 ± 0.14	0.81 ± 0.16
$a_{20}(60)$	1.23 ± 0.02	2.81 ± 0.21	2.90 ± 0.24	−6.13 ± 0.07	−4.22 ± 0.50	−4.91 ± 0.59
$a_{22}(60)$	0	5.00 ± 0.54	5.26 ± 0.59	0	0.76 ± 0.14	0.80 ± 0.16
$a_{20}(70)$	1.10 ± 0.02	2.22 ± 0.13	2.27 ± 0.15	−4.09 ± 0.03	−2.88 ± 0.25	−3.33 ± 0.29
$a_{22}(70)$	0	3.57 ± 0.29	3.77 ± 0.33	0	0.83 ± 0.14	0.87 ± 0.16
$a_{20}(75)$	1.23 ± 0.02	2.88 ± 0.20	2.97 ± 0.22	−5.11 ± 0.05	−4.15 ± 0.43	−4.68 ± 0.47
$a_{22}(75)$	0	5.87 ± 0.57	6.18 ± 0.61	0	0.54 ± 0.15	0.57 ± 0.16
$a_{20}(77)$	0.86 ± 0.01	1.47 ± 0.08	1.48 ± 0.09	−2.54 ± 0.02	−2.13 ± 0.12	−2.29 ± 0.11
$a_{22}(77)$	0	2.55 ± 0.16	2.65 ± 0.17	0	0.43 ± 0.15	0.48 ± 0.16
$a_{20}(79)$	0.87 ± 0.01	1.51 ± 0.09	1.52 ± 0.09	−2.54 ± 0.02	−2.05 ± 0.12	−2.25 ± 0.12
$a_{22}(79)$	0	2.47 ± 0.16	2.58 ± 0.18	0	0.52 ± 0.15	0.56 ± 0.16
$a_{20}(81)$	0.79 ± 0.01	1.39 ± 0.09	1.40 ± 0.10	−2.18 ± 0.02	−1.64 ± 0.10	−1.84 ± 0.11
$a_{22}(81)$	0	1.86 ± 0.14	1.98 ± 0.18	0	0.66 ± 0.15	0.69 ± 0.16
$a_{20}(82)$	0.73 ± 0.01	1.23 ± 0.09	1.22 ± 0.09	−1.95 ± 0.02	−1.53 ± 0.09	−1.69 ± 0.10
$a_{22}(82)$	0	1.75 ± 0.14	1.85 ± 0.17	0	0.53 ± 0.16	0.56 ± 0.16
$a_{20}(83)$	0.63 ± 0.01	1.07 ± 0.10	1.05 ± 0.10	−1.64 ± 0.01	−1.27 ± 0.09	−1.40 ± 0.09
$a_{22}(83)$	0	1.39 ± 0.15	1.49 ± 0.19	0	0.50 ± 0.17	0.52 ± 0.18
$a_{20}(95)$	0.05 ± 0.01	0.24 ± 0.02	0.25 ± 0.03	−0.16 ± 0.01	−0.15 ± 0.01	−0.16 ± 0.01
$a_{22}(95)$	0	0	0	0	0	0
ρ_0/ns^{-1}	7802.46 ± 0.05	7802.97 ± 0.03	7802.92 ± 0.27	999.23 ± 0.001	999.23 ± 0.001	999.23 ± 0.001
E_0/K	4498 ± 44	4154 ± 13	4222 ± 159	3028 ± 12	3236 ± 37	3326 ± 58
$\rho(95)$/ns^{-1}	0.036 ± 0.004	0.087 ± 0.005	0.074 ± 0.030	0.196 ± 0.003	0.138 ± 0.010	0.108 ± 0.014
η	13.23 ± 2.07	1.52 ± 0.22	1.94 ± 1.14	0.25 ± 0.01	0.51 ± 0.08	0.67 ± 0.13
ϵ	0	0	−0.23 ± 0.56	0	0	0.69 ± 0.31
χ_r^2	1.1854	1.1629	1.1628	1.1822	1.1658	1.1641

ellipsoid with the fastest spinning around *b* ($D_b > D_a = D_c$) rather than one with the slowest spinning around *a* ($D_b = D_c > D_a$). An additional symptom of the inadequacy of the simple cylindrical model is related to the temperature dependence of the recovered diffusion tensor components. In fact we find that, for the rod model, $D_b \simeq D_a = D_c$ (i.e., a nearly spherical rotor) at low temperature, while $D_b > D_a = D_c$ only at high temperatures. On the other hand, for the disk model we find $D_b = D_c > D_a$ at all the temperatures. As an example, using the values in Table 1 and eq 19, we find at $T = 35$ °C, $D_b = 0.016$ ns^{-1}, $D_a = D_c = 0.011$ ns^{-1} for the rod, and $D_b = D_c = 0.027$ ns^{-1}, $D_a = 0.014$ ns^{-1} for the disk, while at $T = 83$ °C, $D_b = 0.102$ ns^{-1}, $D_a = D_c = 0.067$ ns^{-1} for the rod, and $D_b = D_c = 0.113$ ns^{-1}, $D_a = 0.058$ ns^{-1} for the disk. This behavior, which might be in principle connected to the chain flexibility, is certainly inconsistent with the requirement of an effective shape associated with the present models.

By allowing also for the biaxiality of the diffusion tensor (columns 4 and 7 in Table 1), the reduction of the global χ^2 achieved by the introduction of the biaxiality parameter ϵ is different when starting from a distorted rod or from a distorted disk. However it is particularly gratifying to see that all the discrepancies outlined above are removed, and we find $D_b > D_a > D_c$ at all the temperatures for both models, in agreement with our previous qualitative considerations based on the amount of displaced solvent.

In summary, Chl *a* is best described by a distorted disk from the point of view of its static ordering matrix, with the axis *a* being the most aligned, but with the diffusion tensor nearly cylindrical around the *b* axis. Only the full biaxial model is able to overcome these difficulties, even if the correctness of the whole procedure is supported mainly by the convergence of the rod and disk models to the same physical picture, rather than merely on a statistical basis.

In Figures 4 and 5 we compare the ordering and diffusion tensor components obtained by the application of the full biaxial treatment either to the rod or to the disk model. From Figure 4 it is clear that the most ordered axis of Chl *a* is *a* (perpendicular to the porphyrin ring), confirming that, from the orientational point of view, Chl *a* is better described as a slightly distorted disk rather than a strongly biaxial rod. This can be concluded also by comparing, in Figure 6, the order parameters $\langle P_2 \rangle$ and $\langle D^2_{02} \rangle$, obtained from the two different choices of the molecular frame, to the limiting physical value of $\langle D^2_{02} \rangle$ as a function of $\langle P_2 \rangle$.[38] A similar conclusion for the order can be reached also for Chl *a* in Merck 85-1084 nematic using a completely different technique: transient EPR following pulse laser excitation as shown by Kothe et al.[16] Their data are also reported in Figure 6 for comparison. Visualization of the significance of the order parameters in terms of the actual average orientation of the probe molecule is perhaps not obvious. Considering the distorted disk as the most appropriate effective shape of Chl *a*, we thus show in Figure 7a−c the maximum entropy orientational distribution functions $P(\beta, \gamma)$ of Chl *a* in ZLI-1167 at three sample temperatures in the nematic range. This representation shows at once to what extent the *z* axis of

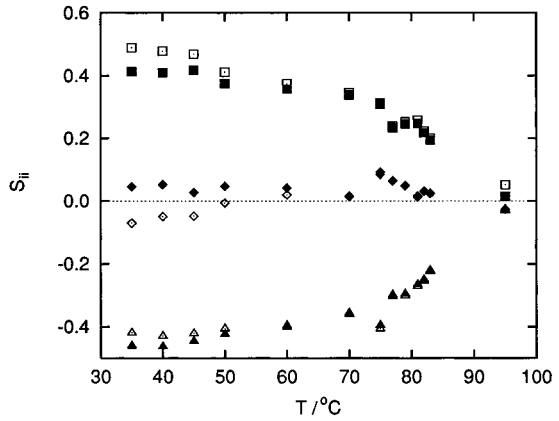

Figure 4. Principal elements S_{ii} of the ordering matrix of Chl *a* in the liquid crystal ZLI-1167, recovered from full biaxial rod (empty symbols) and full biaxial disk (full symbols) models. To make the comparison easier, we have labeled the matrix elements using the same molecular frame *a*, *b*, *c* of Figure 1: (triangles) S_{aa} (S_{yy}, rod; S_{zz}, disk); (squares) S_{bb} (S_{zz}, rod; S_{xx}, disk); (diamonds) S_{cc} (S_{xx}, rod; S_{yy}, disk).

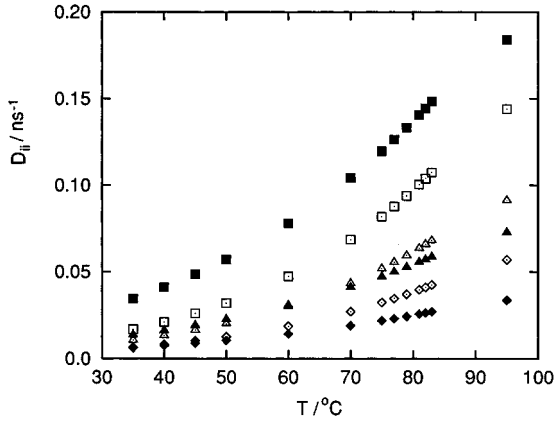

Figure 5. Principal diffusion tensor components D_i of Chl *a* in the liquid crystal ZLI-1167, recovered from full biaxial rod (empty symbols) and full biaxial disk (full symbols) models. Following the same convention of Figure 4, we have labeled the matrix elements using the molecular frame of Figure 1: (triangles) D_a (D_y, rod; D_z, disk); (squares) D_b (D_z, rod; D_x, disk); (diamonds) D_c (D_x, rod; D_y, disk).

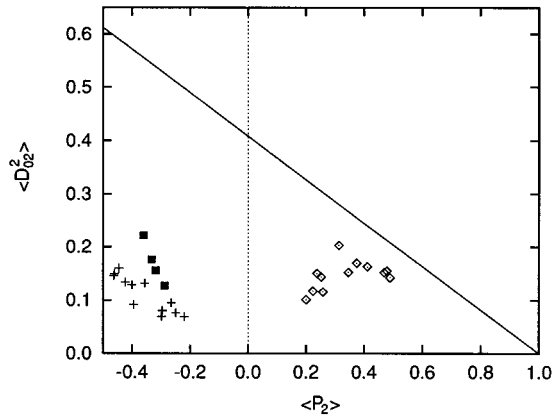

Figure 6. Order parameters $\langle D^2_{02}\rangle$ of Chl *a* in the nematic phase of ZLI-1167 plotted against $\langle P_2\rangle$, obtained from the full biaxial rod (diamonds) and full biaxial disk (crosses) models. Results from Kothe et al.[16] are also reported for comparison (full squares). The continuous line corresponds to the upper physical value[38] of $\langle D^2_{02}\rangle$ as a function of $\langle P_2\rangle$: $\langle D^2_{02}\rangle = [1 - \langle P_2\rangle]/\sqrt{6}$.

Chl *a* is ordered in the liquid crystal and that the rotation around this axis is not isotropic, and thus the molecule is biaxial.

We finally point out that the orientation of the transition moments (see Table 1) is in good agreement with literature values ($\theta_{abs} = 75°$, $\theta_{em} = 57°$).[8d]

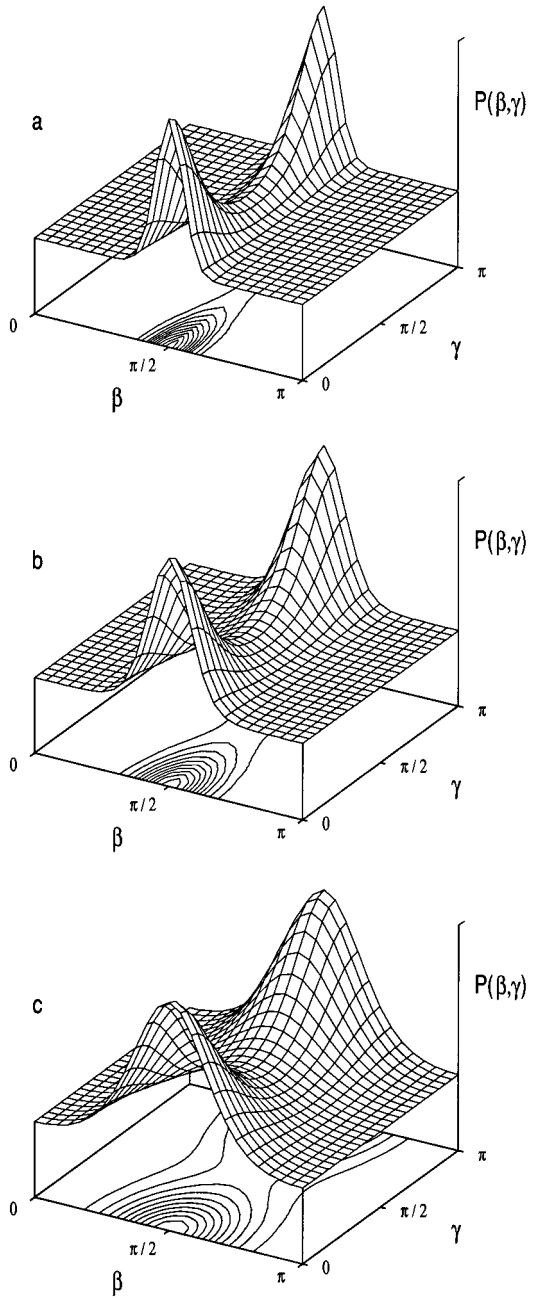

Figure 7. Full biaxial disk orientational distribution functions $P(\beta, \gamma)$ of Chl *a* in ZLI-1167 at three sample temperatures: (a) $T = 35$ °C ($a_{20} = -12.438$, $a_{22} = 0.869$, $\langle P_2\rangle = -0.460$, $\langle D^2_{02}\rangle = 0.150$); (b) $T = 60$ °C ($a_{20} = -4.908$, $a_{22} = 0.802$, $\langle P_2\rangle = -0.400$, $\langle D^2_{02}\rangle = 0.129$); (c) $T = 83$ °C ($a_{20} = -1.402$, $a_{22} = 0.522$, $\langle P_2\rangle = -0.220$, $\langle D^2_{02}\rangle = 0.069$). Contour plots are obtained by sampling the distribution function at 10 equally spaced values between maximum and minimum.

V. Conclusions

Chlorophyll *a* is very well aligned in the nematic liquid crystal ZLI-1167. The axis perpendicular to the porphyrin ring has a strong tendency to be perpendicular to the director with order parameters $S_{aa} < -0.4$ at low temperature, thus approaching the theoretical limiting value of -0.5. The results are also consistent with the qualitative picture obtained from crystallographic methods[2,3] for chlorophyll in membranes. The fluorescence depolarization technique used here can however

give additional information on the deviation from the disklike approximation for Chl *a* and on its dynamics. We have found the ordering matrix of Chl *a* to be strongly biaxial, and allowing for biaxiality in the dynamics as well, we have determined for the first time the rotational diffusion coefficients for the three axes of the molecule. We found the fastest motion to take place around the phytyl chain and the slowest around an axis perpendicular to it while lying in the porphyrin ring plane.

The combination of biaxiality associated with the relative fast dynamics shows that Chl *a* molecules can find themselves on average at a similar orientation so that, for instance, energy transfer might be favored,[6,7] at higher concentrations, even in this low-fluidity system.

Acknowledgment. We are grateful to MURST, University of Bologna, CNR, EU HCM (CT930282), and EU Large Scale Facilities (GE1*CT92-0046) for support of this work. We also thank Prof. S. Califano and Dr. C. Bacchiocchi for stimulating discussions.

References and Notes

(1) Govindjee; Govindjee, R. *Sci. Am.* **1974**, *231*, 68.

(2) Kühlbrandt, W.; Wang, D. N. *Nature* **1991**, *350*, 130.

(3) Krauss, N.; Hinrichs, W.; Witt, I.; Fromme, P.; Pritzkow, W.; Dauter, Z.; Betzel, C.; Wilson, K. S.; Witt, H. T.; Saenger, W. *Nature* **1993**, *361*, 326.

(4) Förster, Th. In *Modern Quantum Chemistry*; Sinanoğlu, O., Ed.; Academic Press: New York, 1965; p 93.

(5) Boulu, L. G.; Kozak, J. J. *Mol. Phys.* **1987**, *62*, 1449.

(6) Bacchiocchi, C.; Zannoni, C. *Chem. Phys. Lett.* **1997**, *268*, 541.

(7) Wagner, R. W.; Johnson, T. E.; Lindsey, J. S. *J. Am. Chem. Soc.* **1996**, *118*, 11166.

(8) (a) van Zandvoort, M. A. M. J.; Wróbel, D.; Scholten, A. J.; de Jager, D.; van Ginkel, G.; Levine, Y. K. *Photochem. Photobiol.* **1993**, *58*, 600. (b) van Zandvoort, M. A. M. J.; Wróbel, D.; Lettinga, P.; van Ginkel, G.; Levine, Y. K. *Photochem. Photobiol.* **1995**, *62*, 279. (c) Wróbel, D.; van Zandvoort, M. A. M. J.; Lettinga, P.; van Ginkel, G.; Levine, Y. K. *Photochem. Photobiol.* **1995**, *62*, 290. (d) van Zandvoort, M. A. M. J.; Wróbel, D.; Lettinga, P.; van Ginkel, G.; Levine, Y. K. *Photochem. Photobiol.* **1995**, *62*, 299. (e) Sanders, R.; van Zandvoort, M. A. M. J.; Draayer, A.; Levine, Y. K.; Gerritsen, H. C. *Photochem. Photobiol.* **1996**, *64*, 817.

(9) (a) van Gurp, M.; van Ginkel, G.; Levine, Y. K. *Biochim. Biophys. Acta* **1988**, *938*, 71. (b) van Gurp, M.; van der Heide, U.; Verhagen, J.; Piters, T.; van Ginkel, G.; Levine, Y. K. *Photochem. Photobiol.* **1989**, *49*, 663.

(10) (a) Chauvet, J. P.; Patterson, L. K. *Thin Solid Films* **1988**, *159*, 149. (b) Boulu, L. G.; Patterson, L. K.; Chauvet, J. P.; Kozak, J. J. *J. Chem. Phys.* **1987**, *86*, 503.

(11) Beddard, G. S.; Porter, G. *Nature* **1976**, *260*, 366.

(12) Katz, J. J.; Shipman, L. L.; Cotton, T. M.; Janson, T. R. In *The Porphyrins*; Dolphin, D., Ed.; Academic Press: New York, 1978; Vol. 5, p 401.

(13) Agostiano, A.; Della Monica, M.; Palazzo, G.; Trotta, M. *Biophys. Chem.* **1993**, *47*, 193.

(14) Frackowiak, D.; Zelent, B.; Malak, H.; Planner, A.; Cegielski, R.; Munger, G.; Leblanc, R. M. *J. Photochem.* **1994**, *78*, 49.

(15) Gonen, O.; Levanon, H. *J. Phys. Chem.* **1984**, *88*, 4223.

(16) Munzenmaier, A.; Rosch, N.; Weber, S.; Feller, C.; Ohmes, E.; Kothe, G. *J. Phys. Chem.* **1992**, *96*, 10645.

(17) Wrobel, D.; Kozielski, M. *Biophys. Chem.* **1988**, *29*, 309.

(18) Subramanian, R.; Patterson, L. K.; Levanon, H. *Photochemistry* **1985**, *41*, 511.

(19) Frackowiak, D.; Bauman, D.; Manikowski, H.; Martynski, T. *Biophys. Chem.* **1977**, *6*, 369.

(20) (a) Frackowiak, D.; Szurkowski, J.; Szych, B.; Hotchandani, S.; Leblanc, R. M. *Photobiochem. and Photobiophys.* **1986**, *12*, 9. (b) Frackowiak, D.; Szurkowski, J.; Hotchandani, S.; Leblanc, R. M. *Mol. Cryst. Liq. Cryst.* **1984**, *111*, 359. (c) Frackowiak, D.; Zelent, B.; Malak, H.; Cegielski, R.; Goc, J.; Niedbalska, M.; Ptak, A. *Biophys. Chem.* **1995**, *54*, 95. (d) Kowalczyk, A.; Zelent, B.; Malak, H.; Planner, A.; Sanocka, S.; Frackowiak, D. *Spectrosc. Lett.* **1996**, *29*, 367.

(21) Bauman, D.; Wrobel, D. *Biophys. Chem.* **1980**, *12*, 83.

(22) O'Connor, D. V.; Phillips, D. *Time-Correlated Single Photon Counting*; Academic Press: London, 1984.

(23) (a) Wedel, H.; Haase, W. *Chem. Phys. Lett.* **1978**, *55*, 96. (b) Pohl, L.; Eidenschink, R.; Krause, J.; Weber, G. Presented at the 7th International Liquid Crystals Conference; Bordeaux, 1978. (c) Merck data sheets.

(24) (a) Arcioni, A.; Bertinelli, F.; Tarroni, R.; Zannoni, C. *Mol. Phys.* **1987**, *61*, 1161. (b) Arcioni, A.; Bertinelli, F.; Tarroni, R.; Zannoni, C. *Chem. Phys.* **1990**, *143*, 259. (c) Arcioni, A.; Tullio, A.; Zannoni, C. *Mol. Cryst. Liq. Cryst.* **1996**, *290*, 255.

(25) Tarroni, R.; Zannoni, C. *J. Chem. Phys.* **1991**, *95*, 4550.

(26) Terpstra, W.; Lambers, W. J. *Photobiochem. Photobiophys.* **1983**, *6*, 93.

(27) Roy, S. *J. Chromatogr.* **1987**, *391*, 19.

(28) Rose, M. E. *Elementary Theory of Angular Momentum*; Wiley: New York, 1957.

(29) (a) Zannoni, C. In *The Molecular Physics of Liquid Crystals*; Luckhurst, G. R., Gray, G. W., Eds.; Academic Press: London, 1979; Chapter 3, p 51. (b) Zannoni, C. In *Polarized Spectroscopy of Ordered Systems*; Samorì, B., Thulstrup, E., Eds.; Kluwer: Dordrecht, 1988; Chapter 3, p 57.

(30) *The Maximum Entropy Formalism*; Levine, R. D., Tribus, M., Eds.; MIT Press: Cambridge, MA, 1979.

(31) (a) Kooyman, R. P. H.; Levine, Y. K.; van der Meer, B. W. *Chem. Phys.* **1981**, *60*, 317. (b) Pottel, H.; Herreman, W.; van der Meer, B. W.; Ameloot, M. *Chem. Phys.* **1986**, *102*, 37.

(32) Arcioni, A.; Tarroni, R.; Zannoni, C. In *Polarized Spectroscopy of Ordered Systems*; Samorì, B., Thulstrup, E., Eds.; Kluwer: Dordrecht, 1988; Chapter 18, p 421.

(33) Zannoni, C. *Mol. Phys.* **1979**, *38*, 1813.

(34) Zannoni, C.; Arcioni, A.; Cavatorta, P. *Chem. Phys. Lipids* **1983**, *32*, 179.

(35) Nordio, P. L.; Segre, U. In *The Molecular Physics of Liquid Crystals*; Luckhurst, G. R., Gray, G. W., Eds.; Academic Press: London, 1979; Chapter 18, p 411.

(36) Huo, S.; Vold, R. R. *J. Phys. Chem.* **1995**, *99*, 12391.

(37) Dong, R. Y.; Shen, X. *J. Chem. Phys.* **1996**, *105*, 2106.

(38) Tarroni, R. Ph.D. Thesis; University of Bologna, 1989.